Engineering Structures 250 (2022) 113371

Contents lists available at ScienceDirect

Engineering Structures

journal homepage: www.elsevier.com/locate/engstruct

A 2.5D coupled FEM–SBM methodology for soil–structure dynamic interaction problems

Hassan Liravi [a,*], Robert Arcos [a,b], Arnau Clot [a,b], Kenny F. Conto [a], Jordi Romeu [a]

[a] Acoustical and Mechanical Engineering Laboratory (LEAM), Universitat Politècnica de Catalunya (UPC). c/ Colom, 11, 08222, Terrassa (Barcelona), Spain
[b] Serra Húnter Fellow, Universitat Politècnica de Catalunya (UPC), Spain

ARTICLE INFO

Keywords:
Soil–structure interaction
Singular boundary method
Finite element method
Elastodynamics
Meshless
Origin intensity factor

ABSTRACT

In this paper, a novel numerical methodology to deal with longitudinally invariant soil–structure interaction problems is proposed. The methodology uses the finite element method to model the structure and the singular boundary method to model the wave propagation in the soil, both formulated in the wavenumber–frequency domain. The versatility presented by the finite element method combined with the simplicity and computational efficiency of the singular boundary method results in a friendly, robust and accurate novel methodology to address the soil–structure interaction problems. The accuracy of the proposed method is assessed by comparing it against 2.5D FEM–MFS and 2.5D FEM–BEM approaches for two cases: a thin cylindrical shell and a star-like beam structure, both embedded in a full-space medium. Moreover, the computational efficiency of the proposed method is evaluated against 2.5D FEM–MFS and 2.5D FEM–BEM methods. In the final step, the applicability of the proposed method is studied through an example of a railway tunnel embedded in a layered half-space. The results presented in this work exhibit the advantages of the novel approach in modelling simplicity, numerical efficiency and robustness with respect to previous methodologies.

1. Introduction

The interest of scientific and technical communities in the dynamic assessment of soil–structure interaction problems has been increasing over the last decade. This area of research covers a wide range of engineering structures [1]. Many of these structures can be assumed to be longitudinally invariant, as it is the case of railway tracks [2], tunnels [2,3], roads [4] and pipelines [5], among others. Thus, the soil–structure interaction for these cases can be assessed by two-and-a-half-dimensional (2.5D) modelling approaches. In past years, there has been an increasing interest in 2.5D modelling approaches due to their merits over three-dimensional (3D) models. The applicability of 2.5D modelling strategies to soil–structure interaction problems was firstly investigated by Hwang et al. [6]. They presented the first work on a 2.5D version of the FEM, along with an application methodology for soil–structure systems. Later, a 2.5D approach based on finite and infinite elements was established by Yang and Hung [7] to model longitudinally invariant unbounded systems subjected to moving loads. In this approach, the infinite elements are used to account for the unbounded domain. It should be noted that a 2.5D FEM approach was presented by Gavríc to compute the dispersion curves associated to longitudinally invariant structures with thin-walled [8] and solid [9] cross sections. A more popular approach to deal with soil–structure interaction problems is the coupled finite element–boundary element method (FEM–BEM), where the FEM is used for modelling the structure and the BEM is used to account for the soil medium. Sheng et al. [10] were the first who worked on a FEM–BEM approach in the context of a 2.5D domain. François et al. [4] proposed a method to use the Green's functions of a layered half-space as fundamental solutions used in the BEM, leading to significant simplifications of the meshing problem. The application of this method in the prediction of railway-induced vibrations is investigated in [2]. Another method to deal with soil–structure interaction problems is proposed by Lopes et al. [11]. They studied the influence of soil stiffness on the soil–structure interaction using the FEM to model the structure together with perfectly matched layers (PML) to account for the unbounded domain of the soil, both formulated in the 2.5D domain. A recent novel approach to study soil–structure interaction systems consisting of a finite structure coupled to a half-space model has been presented by Freisinger et al. [12], in which the soil medium is handled using the integral transform method solution of a half-space with a cylindrical cavity. Then, the structure, modelled using 2.5D finite elements (FE), is coupled in that cavity by soil FE to complete the circular shape.

In order to avoid the constraints due to mesh-based approaches and to increase the computational efficiency of the numerical method,

* Corresponding author.
E-mail address: hassan.liravi@upc.edu (H. Liravi).

https://doi.org/10.1016/j.engstruct.2021.113371
Received 25 May 2021; Received in revised form 18 September 2021; Accepted 12 October 2021

meshless methods have been proposed to model the soil medium in the framework of soil–structure interaction problems. The method of fundamental solutions (MFS) is a meshless method that has been proposed by several authors as an interesting alternative for dealing with these kinds of problems [13–15]. The MFS constructs a set of virtual forces, computed by complying with a particular boundary condition, to obtain an equivalent representation of the structure on the medium. This method is especially interesting for dealing with wave propagation problems in unbounded or partially unbounded domains. In this regard, Amado-Mendes et al. [14] proposed a 2.5D FEM–MFS approach for the analysis of soil–structure interaction systems, in where they used the MFS to compute the soil stiffness matrix required for the dynamic coupling between the soil and the structure. However, MFS accuracy is subjected to the distribution of virtual sources (or virtual forces, in elastodynamics), particularly in terms of amount and location, being this the major challenge of using this approach. To overcome this drawback, Liravi et al. [15] proposed a 2.5D FEM–BEM–MFS approach which uses the BEM to obtain the soil stiffness matrix (MFS still stands for the wave propagation part) and also presents a control methodology to reduce the existing errors associated with the MFS predictions. However, both FEM–MFS and FEM–BEM–MFS methods exhibit complications dealing with complex boundary shapes, due to the difficulties arising in the selection of virtual sources distribution for these geometries. In order to address this MFS drawback, the source points can be relocated on the boundary, overlapping the collocation points. Although this technique eliminates the difficulties with the distribution of the source points, it arises the singularities of the fundamental solutions on the boundary due to the overlap between collocation points and virtual forces. Thus, a regularisation technique should be adopted to overcome these singularities. Young and his colleagues [16] firstly proposed the regularised meshless method (RMM) and Liu [17] further developed it by proposing the double layer potential as the fundamental solution on the basis of the null-field boundary integral equation. Other techniques propose to replace the concentrated source with circular distributed sources [18,19]. In this context, the singular boundary method (SBM) is a novel and emerging meshless boundary collocation method for the solution of the boundary value problems firstly presented by Chen et al. [20]. This method inherits some of the key advantages of the boundary element method (BEM) and the method of fundamental solutions (MFS). On the one hand, the integration procedure that is computationally expensive in BEM-based methods is avoided. On the other hand, the difficulties associated with the source points distribution in MFS are solved by locating the source points on the boundary domain directly. The singularities of the fundamental solutions due to the overlapping between collocation and source points are removed by introducing the concept of origin intensity factor (OIF). In Dirichlet boundary conditions, the OIF can be derived directly as an average value of the fundamental solutions over a portion of the boundary [21]. For Neumann boundary conditions, it can be derived by using a subtracting and adding-back technique [22]. It is worth noting that in most original SBM formulations, single layer potential is employed to overcome those singularities [17]. The original SBM has been reformulated in various works to be adapted to particular cases. An improved singular boundary formulation that uses an inverse interpolation technique to overcome the singularity is presented by Chen et al. [23]. Moreover, asymmetric formulation of the SBM is proposed for problems with mixed boundary conditions. This type of formulation, not only improves the computational efficiency but also enhances the stability of the method [24]. Fu et al. developed a SBM formulation to study acoustic radiation [25] which is recently adapted to deal with periodic systems [26] and to 2.5D problems [27]. Most recently, these authors developed a 3D coupled FEM–SBM approach to address acoustic radiation problems for underwater acoustics [28].

In this paper, a 2.5D FEM–SBM numerical method for longitudinally invariant soil–structure interaction problems is proposed. In this method, the structure is modelled using the 2.5D FEM and a 2.5D SBM approach is adopted to model the surrounding soil. Due to the previously discussed benefits of the SBM with respect to the BEM and the MFS to model unbounded domains, the proposed 2.5D FEM–SBM method exhibits advantages with respect to FEM–BEM and FEM–MFS approaches: modelling simplicity, numerical efficiency and robustness. These benefits are evaluated, analysed and described in this paper. In the 2.5D SBM approach adopted in the present work, the OIFs for Neumann boundary conditions are obtained by using a subtracting and adding-back technique and the OIFs for Dirichlet boundary conditions are obtained by averaging the fundamental solution over a portion of the boundary around the singularity.

The paper is organised as follows. In Section 2, the proposed formulation of the novel 2.5D FEM–SBM approach is presented in detail. Section 3 presents a verification study of the novel method, assessed in the context of two examples: a thin cylindrical shell and a solid beam with star-like cross section, both embedded in a homogeneous full-space. These two examples were selected in order to show the versatility of the method. In the first example, the accuracy of the 2.5D FEM–SBM in terms of the response of the system at the soil–structure boundary and in the soil medium is compared to the responses provided by 2.5D FEM–MFS [14] and 2.5D FEM–BEM [4] approaches. In the second example, the 2.5D FEM–MFS approach is not used in the comparison due to the complexity of the auxiliary boundary definition. A case where the soil and the structure have the same properties is also considered in this second example, allowing for a direct comparison against the elastodynamic fundamental solution of a homogeneous full-space. Moreover, the computational efficiency of the proposed method is evaluated in the context of the first calculation example. Afterwards, in Section 4, the applicability of the proposed method for railway-induced vibration assessment problems is discussed through an example of a railway tunnel embedded in a half-space.

2. Numerical method formulation

Fig. 1 generally illustrates the methodology proposed in the present article. The proposed method is developed to address 2.5D dynamic soil–structure interaction problems. The method considers that the whole system can be divided into two distinct domains, the structure and the soil, each one of them modelled using a different approach: The structure is modelled using the FEM and the unbounded domain representing the soil is modelled by the SBM. In Fig. 1, these sub-systems are denoted by the domains Ω_s (structure) and Ω (soil). The SBM method approximates the solution of the displacement and traction fields at Ω using a set of virtual sources placed along the boundary Γ that comply with the boundary conditions evaluated in the collocation points, which are also distributed along Γ. The coupling between the two subsystems is done by a compatibility of displacements and tractions on the boundary. In this work, the set of FEM nodes on the boundary, collocation points and virtual sources are geometrically coincident, as shown in Fig. 1, which strongly simplifies the coupling procedure. The detailed formulations for the 2.5D SBM and its coupling with the 2.5D FEM are presented in Sections 2.1 and 2.2, respectively. In this work, matrices are denoted by upper case upright bold letters and vectors are denoted by upper case bold italic letters. Moreover, the bar notation represents variables in the wavenumber–frequency domain, where the dynamic Green's functions are represented with bar notation and static Green's functions are represented without bar notation.

2.1. The 2.5D singular boundary method (2.5D SBM)

Using a radial basis function interpolation, the displacement and traction of the soil are approximated by the following linear combination of fundamental solutions with respect to N different source points:

$$\bar{\boldsymbol{U}}(\boldsymbol{y}, k_x, \omega) = \sum_{n=1}^{N} \bar{\mathbf{H}}(\boldsymbol{y}, \boldsymbol{x}^n, k_x, \omega)\bar{\boldsymbol{S}}_n(k_x, \omega), \tag{1}$$

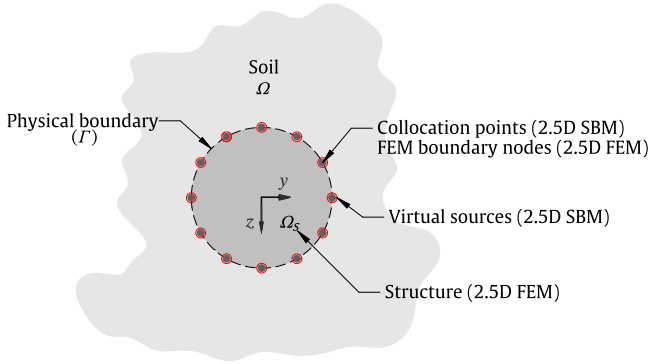

Fig. 1. General description of the proposed 2.5D FEM–SBM methodology. Collocation points and FEM boundary nodes are denoted by grey solid points and virtual forces are denoted by red circles.

$$\bar{\boldsymbol{T}}(\boldsymbol{y},k_x,\omega)=\sum_{n=1}^{N}\bar{\mathbf{H}}^{\tau}(\boldsymbol{y},\boldsymbol{x}^n,k_x,\omega)\bar{\boldsymbol{S}}_n(k_x,\omega) \tag{2}$$

where $\bar{\boldsymbol{U}}(\boldsymbol{y},k_x,\omega)$ and $\bar{\boldsymbol{T}}(\boldsymbol{y},k_x,\omega)$ are the displacements and tractions of the soil, respectively, at an arbitrary field point located at $\boldsymbol{y}$, $\bar{\boldsymbol{S}}_n(k_x,\omega)$ is the vector of unknown strengths of the nth virtual source located at $\boldsymbol{x}^n$ (being n the subscript/superscript used in Eqs. (1) and (2)), and where $\bar{\mathbf{H}}(\boldsymbol{y},\boldsymbol{x}^n,k_x,\omega)$ and $\bar{\mathbf{H}}^{\tau}(\boldsymbol{y},\boldsymbol{x}^n,k_x,\omega)$ are the displacement and traction dynamic Green's functions of the soil considering a point load applied at $\boldsymbol{x}^n$. For clarity, the wavenumber and frequency dependencies will be omitted in the remaining of the paper. For longitudinally invariant structures, the solution of the 3D elastodynamic problem can be expressed in the 2.5D domain. This transformation is derived, for example, in [14], and it is not repeated here for the sake of brevity. Accounting for the 2.5D framework, $\boldsymbol{x}^n$ $\boldsymbol{y}$ are vectors of two elements, while $\bar{\boldsymbol{U}}(\boldsymbol{y})$, $\bar{\boldsymbol{T}}(\boldsymbol{y})$ and $\bar{\boldsymbol{S}}_n$ have three elements, collecting the three components in space of the displacements, tractions and virtual forces, respectively. To evaluate the source strengths, the SBM, as other boundary-type collocation methods, discretises the boundary conditions in a set of points, called collocation points, distributed along the boundary. Then, Eqs. (1) and (2) are used to relate the response at the collocation points with the strengths of all virtual sources. These strengths are finally determined solving the resulting system of equations.

In contrast to the assumptions considered in the MFS, the SBM method assumes that both the collocation and source points are all placed in the same physical boundary, and there is no need of defining a virtual boundary. To avoid the singularities that arise from this assumption when Eqs. (1) and (2) are employed to evaluate the solution on a set of collocation points geometrically coincident with the set of virtual sources, the SBM method assumes that these equations can be rewritten as follows [29]

$$\bar{\boldsymbol{U}}(\boldsymbol{y}^m)=\sum_{n=1,n\neq m}^{N}\bar{\mathbf{H}}(\boldsymbol{y}^m,\boldsymbol{x}^n)\bar{\boldsymbol{S}}_n+\bar{\mathbf{H}}_{mm}\bar{\boldsymbol{S}}_m, \tag{3}$$

$$\bar{\boldsymbol{T}}(\boldsymbol{y}^m)=\sum_{n=1,n\neq m}^{N}\bar{\mathbf{H}}^{\tau}(\boldsymbol{y}^m,\boldsymbol{x}^n)\bar{\boldsymbol{S}}_n+\bar{\mathbf{H}}^{\tau}_{mm}\bar{\boldsymbol{S}}_m, \tag{4}$$

where $\boldsymbol{y}^m$ is the location of the mth collocation point and where $\bar{\mathbf{H}}_{mm}$ and $\bar{\mathbf{H}}^{\tau}_{mm}$ are defined as the origin (or source) intensity factors (OIF) in the SBM literature. A considerable number of numerical and analytical methods have been used to compute the OIF for different types of problems. In the following, the expression of the OIF used in this work is derived.

The OIF associated with the Neumann boundary condition is obtained by applying a subtracting and adding-back technique [30] to Eq. (2). The resulting expression can be written as

$$\begin{aligned}\bar{\boldsymbol{T}}(\boldsymbol{y}^m)=&\sum_{n=1}^{N}\bar{\mathbf{H}}^{\tau}(\boldsymbol{y}^m,\boldsymbol{x}^n)\left(\bar{\boldsymbol{S}}_n-\frac{L_n}{L_m}\bar{\boldsymbol{S}}_m\right)\\&+\left[\sum_{n=1}^{N}\frac{L_n}{L_m}\left(\bar{\mathbf{H}}^{\tau}(\boldsymbol{y}^m,\boldsymbol{x}^n)-\mathbf{H}^{\tau}(\boldsymbol{y}^m,\boldsymbol{x}^n)\right)\right]\bar{\boldsymbol{S}}_m\\&+\left[\sum_{n=1}^{N}\frac{L_n}{L_m}\left(\mathbf{H}^{\tau}(\boldsymbol{y}^m,\boldsymbol{x}^n)+\mathbf{H}^{\tau,I}(\boldsymbol{x}^n,\boldsymbol{y}^m)\right)\right]\bar{\boldsymbol{S}}_m\\&-\left[\sum_{n=1}^{N}\frac{L_n}{L_m}\mathbf{H}^{\tau,I}(\boldsymbol{x}^n,\boldsymbol{y}^m)\right]\bar{\boldsymbol{S}}_m,\end{aligned} \tag{5}$$

where L_i is the half length of the curve between the source points $\boldsymbol{x}^{i-1}$ and $\boldsymbol{x}^{i+1}$, which is approximated in this work as

$$L_i=\frac{d\left(\boldsymbol{x}^{i-1},\boldsymbol{x}\right)}{2}+\frac{d\left(\boldsymbol{x},\boldsymbol{x}^{i+1}\right)}{2}, \tag{6}$$

where $d(x,y)$ refers to the Euclidean distance between points x and y.

In Eq. (5), the terms $\mathbf{H}^{\tau}(\boldsymbol{y}^m,\boldsymbol{x}^n)$ and $\mathbf{H}^{\tau,I}(\boldsymbol{y}^m,\boldsymbol{x}^n)$ are the Green's functions for the traction of the plane strain elastostatic case in the exterior and interior domains, respectively. These two fundamental solutions are related as follows [31]

$$\begin{cases}\mathbf{H}^{\tau}(\boldsymbol{y}^m,\boldsymbol{x}^n)=-\mathbf{H}^{\tau,I}(\boldsymbol{y}^m,\boldsymbol{x}^n), & \text{if} \quad \boldsymbol{x}^n\neq\boldsymbol{y}^m,\\ \mathbf{H}^{\tau}(\boldsymbol{y}^m,\boldsymbol{x}^n)=\mathbf{H}^{\tau,I}(\boldsymbol{y}^m,\boldsymbol{x}^n), & \text{if} \quad \boldsymbol{x}^n=\boldsymbol{y}^m.\end{cases} \tag{7}$$

Defining [29,32]

$$\begin{aligned}\mathbf{A}_m&=L_m\left[\mathbf{H}^{\tau}(\boldsymbol{y}^m,\boldsymbol{x}^m)+\mathbf{H}^{\tau}(\boldsymbol{x}^m,\boldsymbol{y}^m)\right]\\&\approx\int_{\Gamma_m}\left[\mathbf{H}^{\tau}(\boldsymbol{y}^m,\boldsymbol{x})+\mathbf{H}^{\tau}(\boldsymbol{x},\boldsymbol{y}^m)\right]\mathrm{d}\Gamma_m(\boldsymbol{x}),\end{aligned} \tag{8}$$

where Γ_m is the segment of the boundary with length L_m on which the mth collocation point is located, and where the integration is applied componentwise (i.e. the integration is performed for each component of the matrix) and using the relations given by Eqs. (7) and (8), Eq. (5) can be expressed as

$$\begin{aligned}\bar{\boldsymbol{T}}(\boldsymbol{y}^m)=&\sum_{n=1,n\neq m}^{N}\bar{\mathbf{H}}^{\tau}(\boldsymbol{y}^m,\boldsymbol{x}^n)\bar{\boldsymbol{S}}_n-\left[\sum_{n=1,n\neq m}^{N}\frac{L_n}{L_m}\mathbf{H}^{\tau}(\boldsymbol{y}^m,\boldsymbol{x}^n)\right]\bar{\boldsymbol{S}}_m\\&+\frac{1}{L_m}\mathbf{A}_m\bar{\boldsymbol{S}}_m-\left[\sum_{n=1}^{N}\frac{L_n}{L_m}\mathbf{H}^{\tau,I}(\boldsymbol{x}^n,\boldsymbol{y}^m)\right]\bar{\boldsymbol{S}}_m.\end{aligned} \tag{9}$$

The previous expression can be further simplified using that

$$\sum_{n=1}^{N}\frac{L_n}{L_m}\mathbf{H}^{\tau,I}(\boldsymbol{x}^n,\boldsymbol{y}^m)=-\frac{1}{L_m}\mathbf{I}, \tag{10}$$

where $\mathbf{I}$ is the identity matrix. Eq. (10), which has been derived in Appendix, can be used to rewrite Eq. (9) as

$$\begin{aligned}\bar{\boldsymbol{T}}(\boldsymbol{y}^m)=&\sum_{n=1,n\neq m}^{N}\bar{\mathbf{H}}^{\tau}(\boldsymbol{y}^m,\boldsymbol{x}^n)\bar{\boldsymbol{S}}_n\\&+\left[\frac{1}{L_m}\mathbf{I}+\frac{1}{L_m}\mathbf{A}_m-\sum_{n=1,n\neq m}^{N}\frac{L_n}{L_m}\mathbf{H}^{\tau}(\boldsymbol{y}^m,\boldsymbol{x}^n)\right]\bar{\boldsymbol{S}}_m.\end{aligned} \tag{11}$$

The term in brackets can be identified as the OIF for the Neumann boundary conditions defined in Eq. (4), i.e.

$$\bar{\mathbf{H}}^{\tau}_{mm}=\frac{1}{L_m}\left[\mathbf{I}+\mathbf{A}_m-\sum_{n=1,n\neq m}^{N}L_n\mathbf{H}^{\tau}(\boldsymbol{y}^m,\boldsymbol{y}^n)\right]. \tag{12}$$

In the case of the OIF associated to the Dirichlet boundary condition, the singularity that arises is weak (its order being $\ln r$). Due to this, the OIF associated to the mth collocation point can be directly calculated as an average value of the fundamental solution over Γ_m, i.e. the small portion of the boundary that contains the singular point [29]. In this work, this portion of the boundary is approximated by the union of two straight segments, i.e. $\Gamma_m\approx[(\boldsymbol{x}^{m-1}+\boldsymbol{x}^m)/2,\boldsymbol{x}^m]\cup[\boldsymbol{x}^m,(\boldsymbol{x}^m+\boldsymbol{x}^{m+1})/2]$. The integral in Eq. (8) which allows to estimate the term $\mathbf{A}_m$ is computed using the same integration scheme.

2.2. Coupling between the structure and the soil

Consider the radiation problem, where the external loads are applied to the structure. Eqs. (3) and (4) can be rewritten to account for all collocation points in a compact matrix form, resulting on

$$\bar{\boldsymbol{U}}_b = \bar{\mathbf{H}}_{bb}\bar{\boldsymbol{S}}, \quad \bar{\boldsymbol{T}}_b = \bar{\mathbf{H}}^{\tau}_{bb}\bar{\boldsymbol{S}}, \tag{13}$$

where $\bar{\boldsymbol{U}}_b$ and $\bar{\boldsymbol{T}}_b$ are vectors that collect the displacements and tractions at the degrees of freedom of all collocation points, respectively, having a total size $3N$, $\bar{\boldsymbol{S}}$ collects the three components of all virtual forces and $\bar{\mathbf{H}}_{bb}$ and $\bar{\mathbf{H}}^{\tau}_{bb}$ are square matrices containing the displacement and traction dynamic Green's functions (which are simply fundamental solutions when full-space models of the soil are considered [33]) that relate all virtual forces with all collocation points degrees of freedom. Due to the procedure presented in the previous section, no singularities arise on the computation of the $\bar{\mathbf{H}}_{bb}$ and $\bar{\mathbf{H}}^{\tau}_{bb}$ matrices. Note that these matrices directly collect the Green's functions along the boundary, and they are different to the typical BEM square matrices, which are determined integrating the displacement and traction Green's functions on the boundary elements [4]. Thus, the global soil stiffness matrix seen by the structure at the FEM boundary nodes can be consequently written as

$$\bar{\mathbf{K}}_s = \boldsymbol{\Phi}\bar{\mathbf{H}}^{\tau}_{bb}\bar{\mathbf{H}}^{-1}_{bb}, \tag{14}$$

where $\boldsymbol{\Phi}$ is the transformation matrix that converts the unknown nodal tractions on the collocation points to nodal forces. These transformation matrix is defined by

$$\boldsymbol{\Phi} = \int_{\Gamma} \mathbf{N}_b^T \mathbf{N}_b \mathrm{d}\Gamma, \tag{15}$$

where $\mathbf{N}_b$ is the matrix of the global shape functions that discretise the displacements and the tractions on the boundary to the collocation points. Once the soil stiffness matrix is obtained, it can be introduced to the finite element equilibrium equation of the structure, resulting on [4]

$$\left[\mathbf{K}_0 - \mathrm{i}k_x\mathbf{K}_1 + k_x^2\mathbf{K}_2 + \bar{\mathbf{K}}_s - \omega^2\mathbf{M}\right]\bar{\boldsymbol{U}} = \bar{\boldsymbol{F}}, \tag{16}$$

where k_x is the wavenumber, ω is the frequency, $\mathbf{K}_0$, $\mathbf{K}_1$, $\mathbf{K}_2$ and $\mathbf{M}$ are the stiffness and mass matrices associated to the 2.5D FEM model of the structure and $\bar{\mathbf{K}}_s$ is the dynamic stiffness matrix of the soil obtained from the 2.5D SBM model. The stiffness of the soil is frequency and wavenumber dependent, while the stiffness and mass matrices related to FEM domain are not. Vectors $\bar{\boldsymbol{U}}$ and $\bar{\boldsymbol{F}}$ collect nodal displacements and forces, respectively, in all the degrees of freedom of the FEM model. In contrast to the formulation of the 2.5D FEM–MFS approach presented in [14], the present method leads to a symmetric matrix of the coupled system.

The displacements on the collocation points $\bar{\boldsymbol{U}}_b$ due to external forces applied to the structure can be determined using Eq. (16). Then, the corresponding virtual forces to that displacement field on the boundary can be determined by

$$\bar{\boldsymbol{S}} = \bar{\mathbf{H}}^{-1}_{bb}\bar{\boldsymbol{U}}_b. \tag{17}$$

Once the source strengths are computed, the displacement and traction response at an arbitrary field point on the soil can be computed by means of

$$\bar{\boldsymbol{U}}_f = \bar{\mathbf{H}}_{fb}\bar{\boldsymbol{S}}, \quad \bar{\boldsymbol{T}}_f = \bar{\mathbf{H}}^{\tau}_{fb}\bar{\boldsymbol{S}}, \tag{18}$$

where $\bar{\mathbf{H}}_{fb}$ and $\bar{\mathbf{H}}^{\tau}_{fb}$ represent the matrices of source–receiver dynamic Green's functions for displacements and tractions, respectively, and $\bar{\boldsymbol{U}}_f$ and $\bar{\boldsymbol{T}}_f$ stand for the displacement and traction at the field point, respectively.

In the present approach, the 2.5D elastodynamic fundamental solutions for a homogeneous full-space can be calculated with the formulation presented by Tadeu and Kausel [34] and extended by [35], while the Green's functions for homogeneous and layered half-space problems can be computed through the EDT toolbox [36], the approach proposed by Noori et al. [37] or the thin-layer method [38], although other alternative method could be also fully adequate.

3. Verification and computational efficiency assessment

The accuracy of the proposed methodology is exhibited in this section for the two cases presented in Fig. 2(a) and Fig. 2(b). As illustrated, the structures of these two cases consist of a thin cylindrical shell and a solid beam with star-like cross section, respectively, both embedded in a full-space model of the soil. The results obtained using the proposed 2.5D FEM–SBM methodology are compared with those obtained using a 2.5D FEM–MFS [14] approach, only in the case of the thin cylindrical shell, and a 2.5D FEM–BEM [4] approach. In boundary methods, accuracy on the method strongly relies on the accuracy of the boundary condition. Thus, the responses are firstly compared on the physical boundary of the structure in the thin cylindrical shell example. For the sake of certainty, the responses at different field points in the soil have been also compared. The system's symmetry has been taken into account when presenting the boundary results. Therefore, results for only half of the boundary have been presented in the plots. In the star-like solid beam structure example, the results are compared in the same field points in the soil considered in the case of the cylindrical shell.

The comparison between the three numerical approaches is performed in terms of receptances and traction transfer functions (TTF) computed in the frequency domain. In both cases, a harmonic vertical point load is applied on the embedded structure at $x = 0$. The position of the loads within both cross section has been presented in Fig. 2(a) and (b) with a larger grey arrow. In both examples, the soil response has been calculated at three different locations, identified as point A ($x = 0$ m; $y = 2$ m; $z = -2$ m), B ($x = 0$ m; $y = 4$ m; $z = -1$ m) and C ($x = 0$ m; $y = 10$ m; $z = 2$ m). Stating the transformation of an arbitrary response $g(x,t)$ in the space–time domain to the wavenumber–frequency domain on the basis of a double Fourier transform defined by

$$\bar{G}(k_x,\omega) = \int_{-\infty}^{+\infty}\int_{-\infty}^{+\infty} g(x,t)\mathrm{e}^{\mathrm{i}(k_x x-\omega t)}\mathrm{d}x\mathrm{d}t, \tag{19}$$

the receptance and traction transfer functions at $x = 0$ can be obtained from the following inverse Fourier transforms

$$\boldsymbol{U}_f(\omega) = \frac{1}{2\pi}\int_{-\infty}^{+\infty}\bar{\boldsymbol{U}}_f(k_x,\omega)\,\mathrm{d}k_x, \qquad \boldsymbol{T}_f(\omega) = \frac{1}{2\pi}\int_{-\infty}^{+\infty}\bar{\boldsymbol{T}}_f(k_x,\omega)\,\mathrm{d}k_x. \tag{20}$$

Due to the symmetries of the displacements and tractions in the wavenumber–frequency domain due to a vertical load, the x components of the receptances and traction transfer functions for this direction are null at $x = 0$. In contrast, the other components can be computed by

$$U_f^i(\omega) = \frac{1}{\pi}\int_0^{\infty}\bar{U}_f^i(k_x,\omega)\,\mathrm{d}k_x, \qquad T_f^i(\omega) = \frac{1}{\pi}\int_0^{\infty}\bar{T}_f^i(k_x,\omega)\,\mathrm{d}k_x, \quad \text{for } i = y,z \tag{21}$$

where i refers to the component of the receptance or the traction transfer function. In all calculations carried out in this section, both integrals have been computed numerically with a total of 1025 sampling points consisting of $k_x = 0$ and a logarithmically spaced vector of wavenumbers ranging from 10^{-3} to 10^{2} rad/m. For the 2.5D FEM–BEM three Gaussian points are considered. Results for the receptances and the traction transfer functions are presented in dB based on references of 10^{-12} m/N and 1 (N/m^2)/N, respectively.

The results have been obtained considering the following mechanical parameters for the soil: a Young's modulus of 108 MPa, a density of 1800 kg/m^3, a Poisson's ratio of 0.33 and material damping ratio of 0.05. All this verification process has been performed in the frequency range of 0 to 100 Hz.

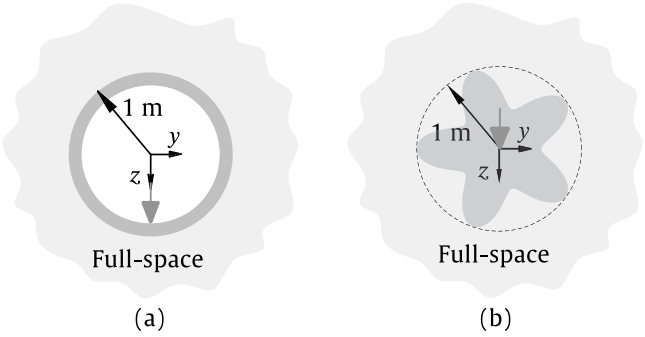

Fig. 2. Geometry of the thin cylindrical shell (a) and the star-like shape (b) used for the comparison between the three methods.

3.1. Thin cylindrical shell

The case studied in this section is presented in Fig. 2(a). The cylindrical shell is assumed to have a thickness of 0.1 m and material properties of a common concrete: a Young's modulus of 31 000 MPa, a density of 2500 kg/m^3, a Poisson's ratio of 0.2 and a material damping ratio of 0.001. Two meshing strategies have been considered to model this system. In the first strategy, the density of the FEM mesh at the boundary has been selected to have at least 10 nodes per wavelength of the soil shear waves at 100 Hz, which is the higher frequency of the range considered. Due to the coupling strategy between the FEM and SBM models adopted in the present methodology, 10 FEM nodes per wavelength at the boundary also implies 10 collocation points and 10 virtual sources per wavelength. In the second case, up to 24 nodes per wavelength have been considered. For these two cases, the results on the boundary are compared with the ones obtained by the 2.5D FEM–BEM and 2.5D FEM–MFS approaches. In the 2.5D FEM–MFS approach, the virtual sources are located outside of the soil domain (i.e. inside the structure domain), uniformly distributed in a concentric circumference to the cylindrical shell. The radius of this auxiliary boundary for the virtual sources has been optimised using the method presented in [15], reaching a value of 85 cm. This optimisation is performed accounting for point B as the control point. In the same way than in the proposed SBM methodology, the FEM–MFS approach has been applied considering the same amount of virtual sources than collocation points.

Results for the cylindrical shell case study are presented in Figs. 3 and 4. Fig. 3 compares the receptances and tractions transfer functions along the soil–structure interface obtained using the three mentioned numerical approaches for the case of 10 collocation points per wavelength and considering two excitation frequencies: 10 Hz and 80 Hz. The results are only compared for y and z components since the displacements and tractions in the x direction are equal to zero. A very good match can be observed between the three methods in the receptance plots. However, for both excitation frequencies, some differences arise between the traction transfer functions obtained with the 2.5D FEM–MFS and the two other methods. It is found that these discrepancies are coming from the instability of the 2.5D MFS method at high wavenumbers. Also, the accuracy of the results is sensitive to the control points chosen in the control technique [15] and, consequently, the location of the virtual sources [39,40]. Fig. 4 shows the comparison between the three numerical approaches for the case 24 collocation points per wavelength. The new results show a good agreement between the three methods in all the cases considered. The discrepancies previously observed for the 2.5D FEM–MFS method have been clearly reduced, a result that suggests that a larger number of collocation points per wavelength should be used in this method.

The accuracy of the presented method is also studied in this section by comparing the soil response obtained using the three numerical approaches previously considered. In this case, the comparison between these methods has been performed computing the soil receptance and traction transfer functions for excitation frequencies ranging from 0 to 100 Hz. The results have been computed for the three field points previously detailed (A, B and C) and considering 10 collocation points per wavelength. The comparisons are presented in Fig. 5, which shows a very good agreement between the three methods for all the cases considered. The results presented in this section in terms of boundary and field displacements and tractions confirm that the proposed method can be used to deal with problems that have geometrically smooth soil–structure interfaces.

The accuracy of the method has been also assessed by comparing the results with an analytical solution in terms of receptances and traction transfer function. In this regard, the calculation has been repeated replacing the concrete material by soil material, allowing to compare the proposed method with the cylindrical cavity solution [41]. According to Fig. 6, good agreement can be observed between the proposed method and the other presented solutions.

Furthermore, the performance of the 2.5D FEM–SBM approach is evaluated by analysing its convergence with respect to 2.5D FEM–BEM and 2.5D FEM–MFS methods. For this aim, the root mean square error of the methods (RMSE) is calculated by using Eq. (23) for the case presented in Fig. 6. The cylindrical cavity solution is adopted as the exact reference solution for the convergence analysis. The receptances at field points A, B and C are computed using the wavenumber sampling previously described. The analysis is carried out based on a number of nodes per wavelength ranging from 6 to 20 with unit intervals. As shown in Fig. 7, the 2.5D FEM–SBM has a better performance than 2.5D FEM–BEM for low frequency (10 Hz) but worsens for higher ones (80 Hz). 2.5D FEM–MFS has proven a potential to be more accurate than the other methods, but it requires a proper optimisation process [15] to determine the sources location, which is challenging (or even impossible) for complex geometries. In contrast, at high frequencies, more than 10 N/λ is required by the 2.5D FEM–SBM approach to achieve approximately one percent error. However, errors achieved by all methods are more than acceptable for engineering applications.

3.2. Star-like shape structure

To demonstrate the generality of the proposed approach, the accuracy of the method is investigated in this section for the case of solid beam with star-like cross section embedded in a full-space, as illustrated in Fig. 2(b). The parametric representation of the star-like shape boundary geometry is

$$\begin{aligned} y &= \frac{1}{m^2}(m^2+2m+2-2(m+1)\cos(m\phi))\cos(\phi), \\ z &= \frac{1}{m^2}(m^2+2m+2-2(m+1)\cos(m\phi))\sin(\phi), \end{aligned} \tag{22}$$

where m represents the shape factor ($m = 5$ is considered in this study) and ϕ denotes the angular coordinate of the polar coordinate system. Two different materials have been considered for the structure in order to perform two comparisons between the proposed 2.5D FEM–SBM method and the 2.5D FEM–BEM method. While in the first comparison the star-like structure is considered to be solid concrete with the same properties of the cylindrical shell presented in the previous section, in the second comparison its mechanical properties are assumed to be the same as those considered for the surrounding soil. Since in this second calculation example both the structure and the soil have the same mechanical properties, the responses obtained by the proposed method can be also compared to the fundamental solution of a homogeneous full-space [34]. For both cases, the comparisons are presented at the same three field points that have been considered in the previous section (field points A, B and C). The results have been computed considering 10 collocation points per wavelength and these points are distributed uniformly along the perimeter of the boundary.

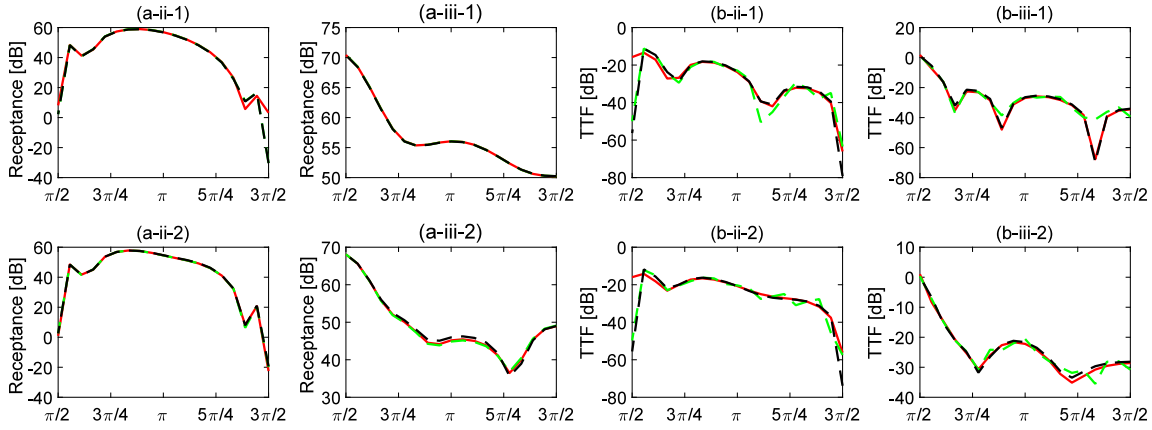

Fig. 3. Receptances (a) and traction transfer functions (b) on the boundary for the case of 10 collocation points per wavelength. Methods: 2.5D FEM–BEM [4] (solid red line), 2.5D FEM–SBM (dashed black line) and 2.5D FEM–MFS [14] (dashed green line). The results are obtained for y (ii) and z (iii) directions at frequencies of 10 Hz (1) and 80 Hz (2). (For interpretation of the references to colour in this figure legend, the reader is referred to the web version of this article.)

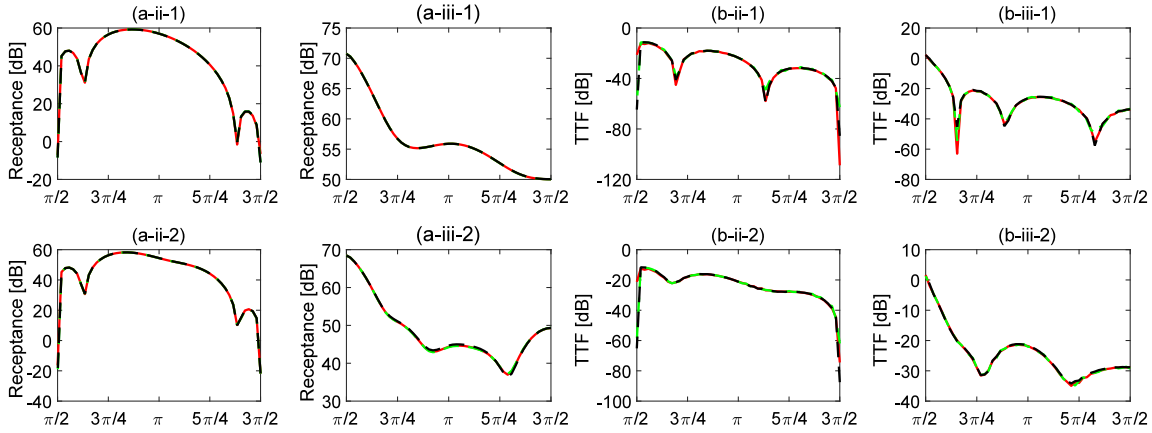

Fig. 4. Receptances (a) and traction transfer functions (b) on the boundary for the case of 24 collocation points per wavelength. Methods: 2.5D FEM–BEM [4] (solid red line), 2.5D FEM–SBM (dashed black line) and 2.5D FEM–MFS [14] (dashed green line). The results are obtained for y (ii) and z (iii) directions at frequencies of 10 Hz (1) and 80 Hz (2). (For interpretation of the references to colour in this figure legend, the reader is referred to the web version of this article.)

Fig. 8 presents a comparison between the results obtained by the novel 2.5D FEM–SBM and the 2.5D FEM–BEM approaches for the case of the concrete star-like structure described previously. The results show that the receptances computed by the proposed method at points A, B and C agree reasonably well with those obtained by the 2.5D FEM–BEM approach. Highest discrepancies up to 0.3 dB are found at the near-field (see Fig. 8 (a-ii)).

Fig. 9 shows the results obtained using the 2.5D FEM–SBM approach for the case where both the structure and the soil have the same mechanical properties. In the case of the receptances, these results are compared with those obtained using the 2.5D FEM–BEM approach and using the elastodynamic fundamental solutions of a homogeneous full-space. For the traction transfer functions, the 2.5D FEM–SBM results are only compared to the fundamental solutions. Good agreements are observed between the 2.5D FEM–SBM results and the results obtained with the other approaches. Only small discrepancies are observed in traction transfer functions in the far-field (see Fig. 9 (c-ii-2)), especially at low frequencies. Therefore, from the results obtained in these two examples, it can be interpreted that the proposed method not only is practical for structures with simple geometries, but also provides good accuracy in cases where geometrically complicated structures are involved.

3.3. Comparison of the relative error between the methods

In the previous sections, the results obtained with the 2.5D FEM–SBM method have been compared to the ones obtained with the 2.5D FEM–BEM and the 2.5D FEM–MFS approaches for two different case studies. Even though the accuracy of the presented method could be inferred from these results, it is desirable to investigate it using more robust indicators. In this section, the accuracy of the new approach is assessed by evaluating the relative errors between all three numerical approaches with respect to the displacement and traction response on the boundary. The comparison is performed considering the case of the thin cylindrical shell embedded in a full-space presented in Section 3.1. It is worth mentioning that the term **A** presented in Eq. (8) has not been used in the calculations described in this section, since this term does not provide significant benefits in terms of accuracy of the results in the case of smooth geometries. The relative errors associated to the displacement and traction fields along the boundary are computed using the following expressions

$$\varepsilon_r = \sqrt{\frac{1}{N}\sum_{j=1}^{N}\left|\frac{\frac{1}{3}\sum_{i=1}^{3}\bar{U}_b^{ij} - \frac{1}{3}\sum_{i=1}^{3}\bar{U}_{br}^{ij}}{\frac{1}{3}\sum_{i=1}^{3}\bar{U}_{br}^{ij}}\right|^2},$$
$$\varepsilon_r^{\tau} = \sqrt{\frac{1}{N}\sum_{j=1}^{N}\left|\frac{\frac{1}{3}\sum_{i=1}^{3}\bar{T}_b^{ij} - \frac{1}{3}\sum_{i=1}^{3}\bar{T}_{br}^{ij}}{\frac{1}{3}\sum_{i=1}^{3}\bar{T}_{br}^{ij}}\right|^2}, \tag{23}$$

where i is the index associated with the coordinate components (x, y and z), j is the index associated to the collocation points and N refers to the total number of collocation points in the model. Moreover, $\bar{U}_b^{ij}$ and $\bar{U}_{br}^{ij}$ represent the displacement Green's functions in the wavenumber–frequency domain on the boundary obtained by the selected method

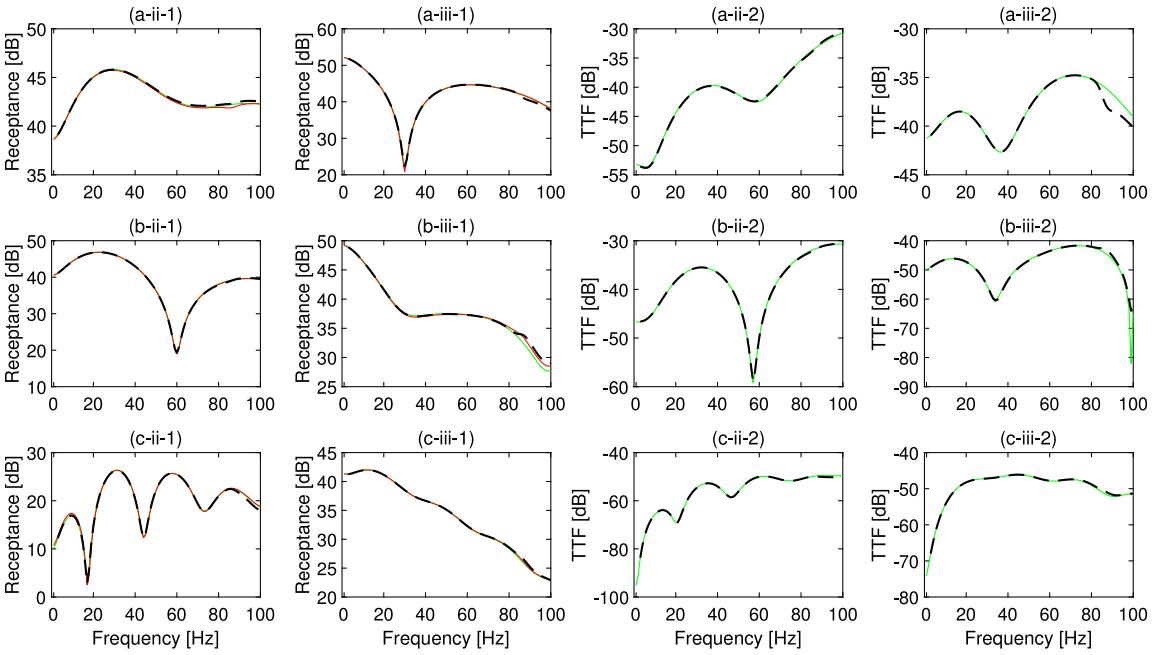

Fig. 5. Receptances (1) and traction transfer functions (2) at the field points A (a), B (b) and C (c) for y (ii) and z (iii) directions and for the case of 10 collocation points per wavelength. Methods: 2.5D FEM–BEM [4] (solid red line), 2.5D FEM–SBM (dashed black line) and 2.5D FEM–MFS [14] (dashed green line). (For interpretation of the references to colour in this figure legend, the reader is referred to the web version of this article.)

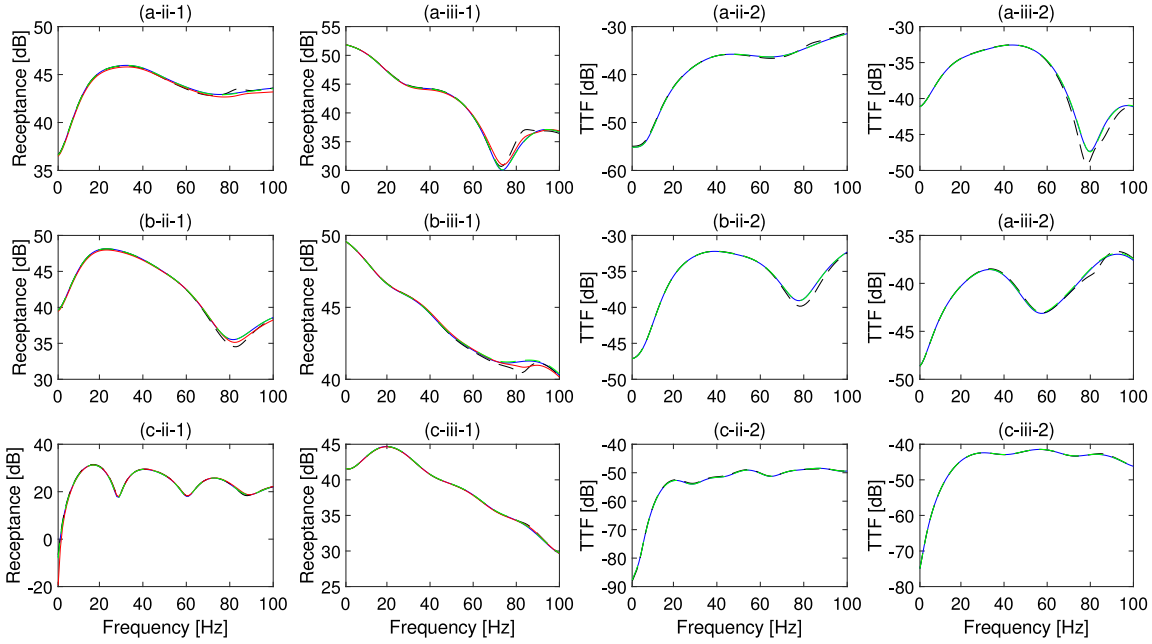

Fig. 6. Receptances (1) and traction transfer functions (2) at the field points A (a), B (b) and C (c) for y (ii) and z (iii) directions and for the case of 10 collocation points per wavelength. Methods: 2.5D FEM–BEM [4] (solid red line), 2.5D FEM–SBM (dashed black line), 2.5D FEM–MFS [14] (dashed green line) and cylindrical cavity solution [41] (solid blue line). (For interpretation of the references to colour in this figure legend, the reader is referred to the web version of this article.)

and by a reference method, respectively, at the collocation point j and in the direction i. Analogously, $\bar{T}_b^{ij}$ and $\bar{T}_{br}^{ij}$ represent the traction Green's functions in the wavenumber–frequency domain on the boundary obtained by the selected method and by a reference method, respectively, at the collocation point j and in the direction i. Both errors have been computed for frequencies between 0 and 100 Hz, for wavenumber values from 0.1 rad/m to 10 rad/m, and considering 10 or 24 collocation points per wavelength.

The colour map plots presented in Fig. 10 show the relative errors obtained when 10 collocation points per wavelength are considered. For clarity, the errors are presented on a logarithmic scale. Also, receptances and traction transfer functions corresponding to these colour maps are also presented, where the relative errors between the methods have been computed using the same expressions than before but replacing the displacement and traction Green's functions with the corresponding transfer function. The results show that the displacement and traction Green's functions obtained by the proposed method converge well to those obtained using the 2.5D FEM–BEM approach. Colour map plots show that the discrepancies between the 2.5D FEM–MFS and the 2.5D FEM–BEM methods at large wavenumbers are significant for

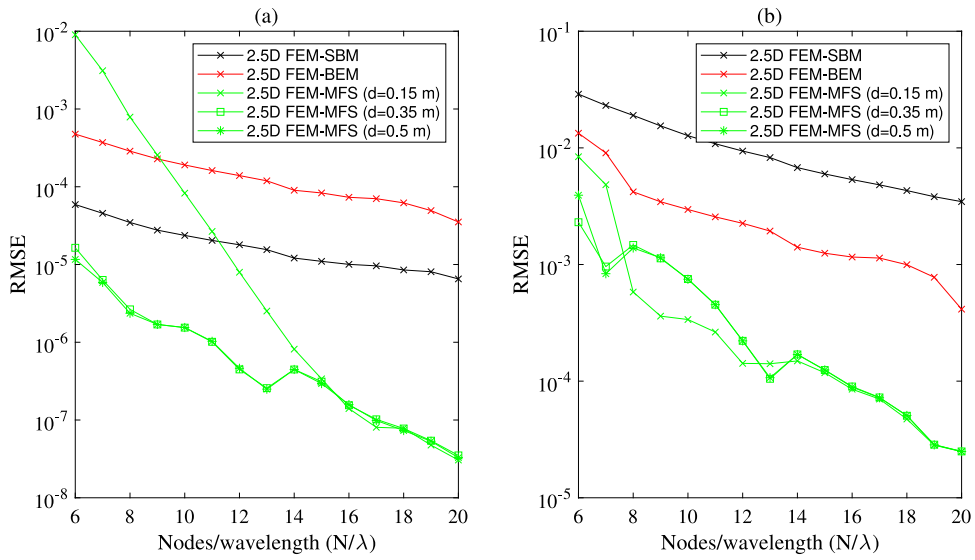

Fig. 7. Convergence analysis for receptances averaged at the three fields points A, B and C and at 10 Hz (a) and 80 Hz (b). (For interpretation of the references to colour in this figure legend, the reader is referred to the web version of this article.)

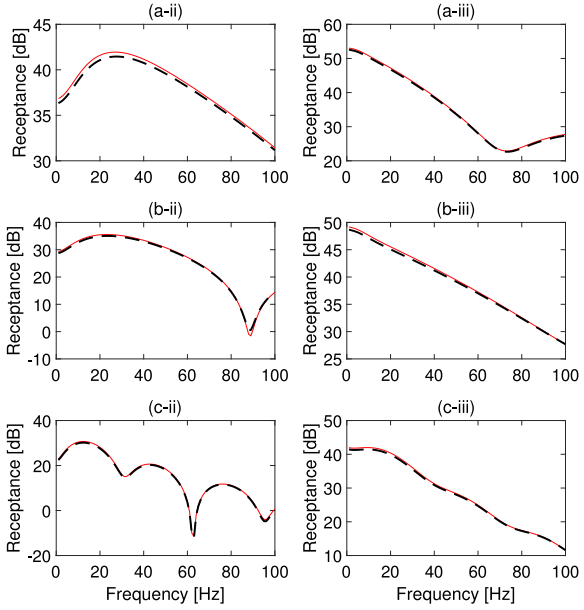

Fig. 8. Receptances at the field points A (a), B (b) and C (c) for y (ii) and z (iii) directions. Methods: 2.5D FEM–BEM [4] (solid red line), 2.5D FEM–SBM (dashed black line).

almost all the range of frequencies, although these discrepancies have a small effect on the receptances and traction transfer functions. The relative errors between the 2.5D FEM–SBM and the 2.5D FEM–BEM approaches associated to the displacements are smaller than the errors between the 2.5D FEM–MFS and the 2.5D FEM–BEM approaches at frequencies between 20 Hz and 80 Hz. In contrast, the opposite trend is observed below 20 Hz and above 80 Hz. However, larger discrepancies are observed in the relative error associated with the traction Green's functions. In this case, the relative errors between the 2.5D FEM–SBM and the 2.5D FEM–BEM approaches are considerably smaller than those found between the 2.5D FEM–MFS and the 2.5D FEM–BEM.

The results previously presented in Section 3.1 showed that the accuracy of the 2.5D FEM–SBM and 2.5D FEM–MFS can be significantly improved by considering a larger number of collocation points per wavelength. Therefore, it is expected that an increase in the number of collocation points should result in a decrease of the relative error between the presented meshless methods and the 2.5D FEM–BEM approach. This hypothesis is confirmed by the results presented in Fig. 11, in which the relative errors between the methods have been calculated considering 24 collocation points per wavelength instead of 10. It can be observed that displacement results exhibit lower discrepancies between the methods, although the accuracy enhancement provided by the use of 24 collocation points per wavelength is not high enough to justify a mesh refinement such as this. The same tendency can be observed for the traction results, for which such a refinement is found to be more important to ensure the 2.5D FEM–MFS proper performance.

3.4. Investigation of the computational efficiency of the method

In this section, the proposed 2.5D FEM–SBM method is compared to the 2.5D FEM–BEM and 2.5D FEM–MFS approaches in terms of computational efficiency. The comparison is performed in the framework of the thin cylindrical shell case study presented in Section 3.1. All three methodologies have been implemented in MATLAB and have been executed using a single core of a high-performance cluster with 2 GHz Intel® Xeon® Gold 6138 CPU (with 40 cores). The computational cost of each one of these methods is evaluated for two different case scenarios. In the first case, the soil responses are computed in a single field point, for a specific frequency, for 1024 wavenumber values and considering different values for the number of collocation points per wavelength: 6, 10, 17 and 24. In the second case, the soil responses are computed for one frequency, 1024 wavenumber samples, 24 collocation points per wavelengths and considering different values for the number of field points: from 5 to 200.

The results obtained in the first case are indicated in Table 1. The computational time spent by the three methods increases quadratically with the number of collocation points per wavelength. However, the slope of this increase for the 2.5D FEM–MFS and 2.5D FEM–SBM approaches is smaller than the one observed for the case of the 2.5D FEM–BEM approach.

The computational times obtained in the second case are presented in Table 2. As in the previous case, a quadratic increase with the number of evaluation points is observed for all three methods. However, in this case the slope of this increase for the 2.5D FEM–BEM approach is much larger than the one observed for the other two approaches. This result shows the clear benefit that the use of 2.5D FEM–MFS or 2.5D FEM–SBM approaches has when the response of a large number of evaluation points is required.

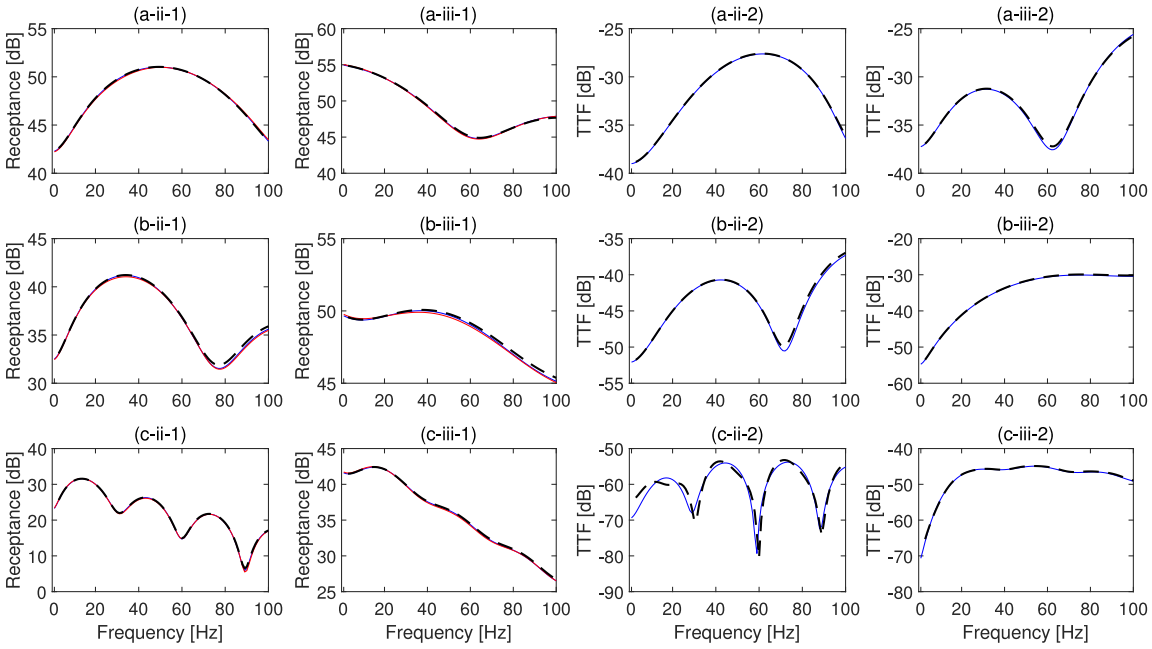

Fig. 9. Receptances (1) and traction transfer functions (2) at the field points A (a), B (b) and C (c) for y (ii) and z (iii) directions. Methods: 2.5D FEM–BEM [4] (solid red line), 2.5D FEM–SBM (dashed black line) and fundamental solution [36] (solid blue line). (For interpretation of the references to colour in this figure legend, the reader is referred to the web version of this article.)

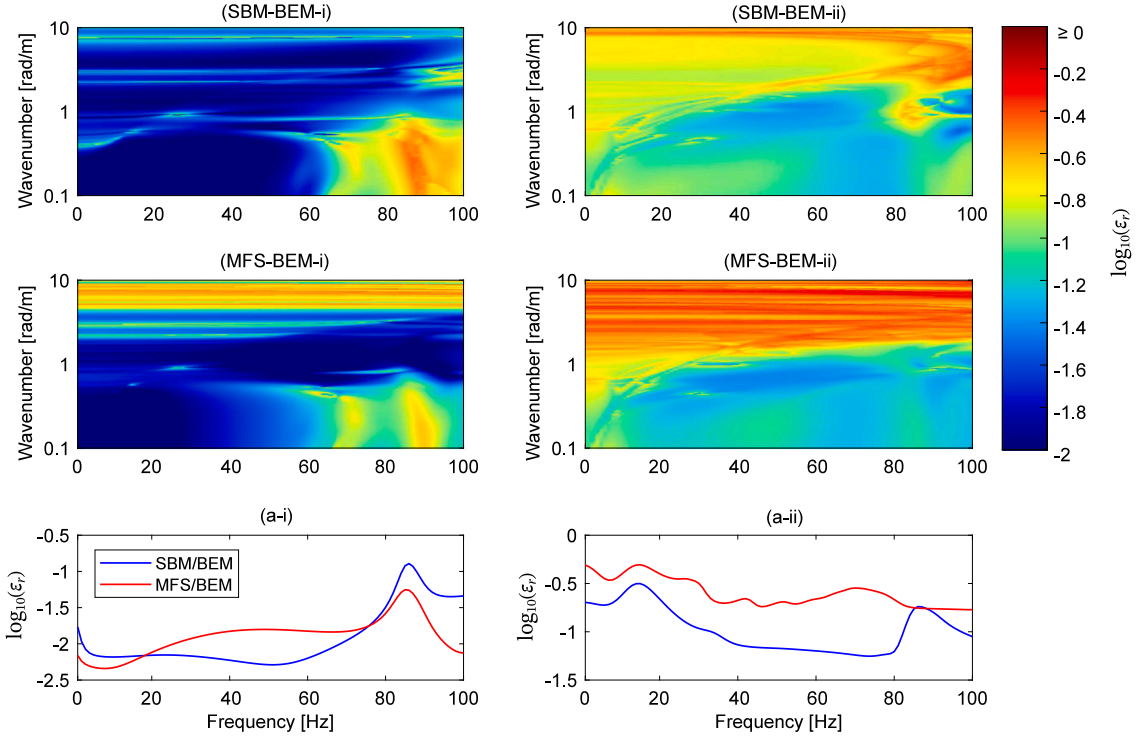

Fig. 10. Relative error of the displacement Green's functions (i) and traction Green's functions (ii) on the boundary considering 10 collocation points per wavelength. Plots denoted by (a-i) and (a-ii) represent the relative error in terms of receptances and traction transfer functions, respectively. SBM/BEM refers to the relative error when the selected method is the 2.5D FEM–SBM and the reference is the 2.5D FEM–BEM [4] approach and MFS/BEM refers to the relative error when the selected method is the 2.5D FEM–MFS [14] and the reference is the 2.5D FEM–BEM one. (For interpretation of the references to colour in this figure legend, the reader is referred to the web version of this article.)

From the results presented in Tables 1 and 2, it can be concluded that the 2.5D FEM–MFS and the 2.5D FEM–SBM approaches can be much more efficient than the 2.5D FEM–BEM approach in many practical scenarios. The comparison also shows that the 2.5D FEM–SBM approach is slightly slower than the 2.5D FEM–MFS approach. This extra computational time spent by the 2.5D FEM–SBM approach comes from the evaluation of the OIF terms.

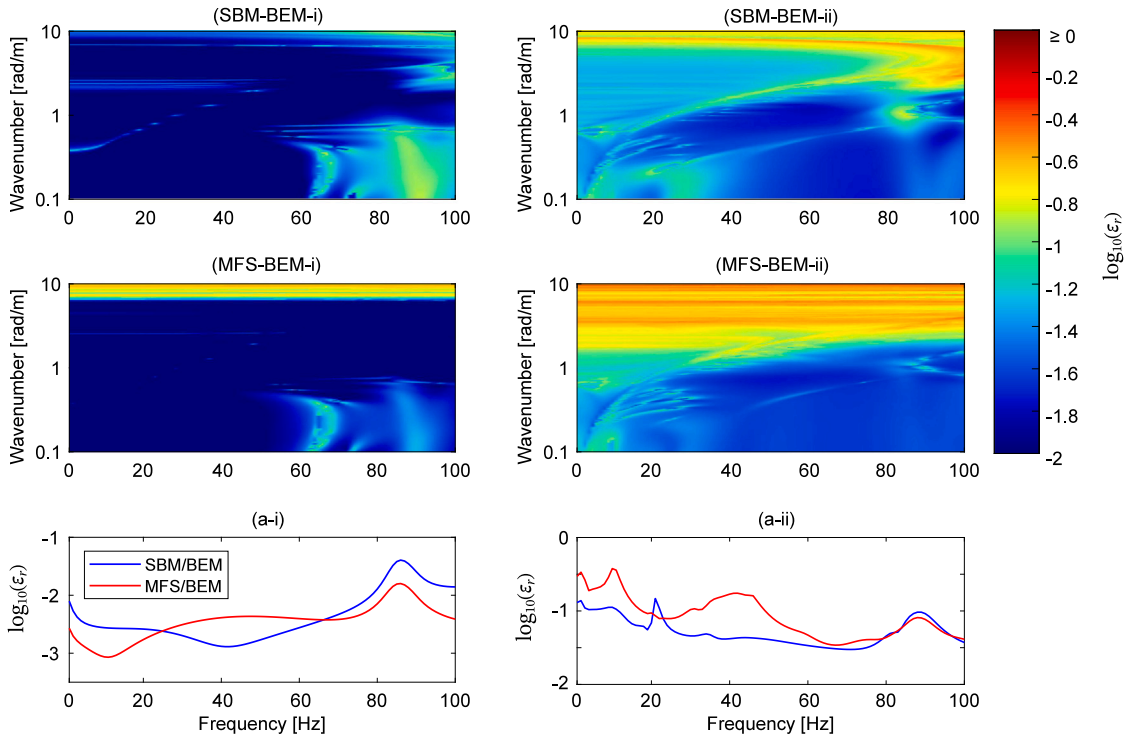

Fig. 11. Relative error of the displacement Green's functions (i) and traction Green's functions (ii) on the boundary considering 24 collocation points per wavelength. Plots denoted by (a-i) and (a-ii) represent the relative error in terms of receptances and traction transfer functions, respectively. SBM/BEM refers to the relative error when the selected method is the 2.5D FEM–SBM and the reference is the 2.5D FEM–BEM [4] approach and MFS/BEM refers to the relative error when the selected method is the 2.5D FEM–MFS [14] and the reference is the 2.5D FEM–BEM one. (For interpretation of the references to colour in this figure legend, the reader is referred to the web version of this article.)

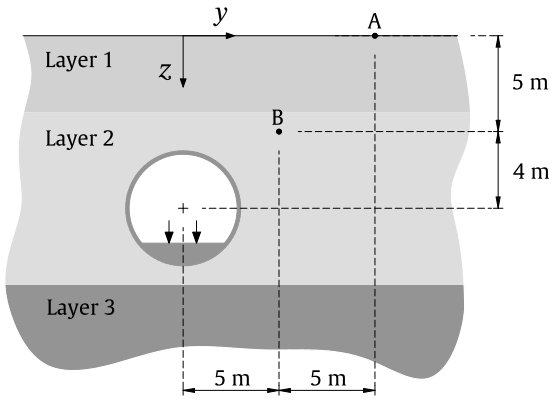

Fig. 12. Geometry of the problem. The position of the forces and the position of the receivers are also presented.

Table 1
Computational costs in seconds of the three methods for different number of collocation points per wavelength.

Number of collocation points per wavelength	6	10	17	24
Computational time using 2.5D FEM–SBM [s]	38	49	84	133
Computational time using 2.5D FEM–MFS [s]	35	44	77	124
Computational time using 2.5D FEM–BEM [s]	43	53	95	163

4. Application to the assessment of railway-induced ground-borne vibrations

4.1. Model description

The numerical implementation and accuracy of the proposed 2.5D FEM–SBM have been fully addressed in the previous sections. The aim of this section is to present an application example of the 2.5D FEM–SBM approach to the assessment of tunnel-soil transfer functions required for railway-induced ground-borne vibration assessment. With the purpose of depicting the potentialities of the proposed method, an underground railway circular tunnel with an external radius of 3 m and a wall thickness of 0.3 m embedded in a layered half-space is considered. The system is illustrated in Fig. 12. The centre of the tunnel is located at a depth of 9 m from the ground surface and the structure is excited by two harmonic point loads symmetrically applied on the tunnel invert and separated 1.5 m. The response of the soil has been calculated at two different evaluation points (identified as A and B), one located on the ground surface and the other within the soil. As before, in this example it is assumed that the evaluation points and the applied point loads are all always in the same cross section. The geometry of the soil–structure system and the location of the two considered evaluation points are presented in Fig. 12. The mechanical properties of the tunnel lining and the soil are presented in Table 3. The FEM mesh, the position of the collocation/source points and the position of the two forces are specified in Fig. 13. Since the frequency range of interest for railway-induced vibration problems is 1–80 Hz [42], the application of the proposed method is evaluated up to 100 Hz. Two FEM meshes have been created to deal with this problem, having 6 and 8 nodes per wavelength (considering a maximum frequency of 100 Hz, as mentioned) along the boundary.

Table 2
Computational costs in seconds of the three methods for different number of field points.

Number of field points	5	25	60	100	160	200
Computational time using 2.5D FEM–SBM [s]	53	56	64	71	82	102
Computational time using 2.5D FEM–MFS [s]	46	50	57	65	75	94
Computational time using 2.5D FEM–BEM [s]	60	102	153	264	461	665

Table 3
Mechanical parameters of the tunnel and the layered soil.

Type	E [MPa]	ρ [kg/m^3]	ν	Thickness [m]	Damping
Tunnel	31 000	2500	0.2	0.3	0.001
Soil layer 1	50	1900	0.3	4	0.05
Soil layer 2	180	1980	0.3	9	0.05
Soil layer 3	400	2050	0.3	∞	0.05

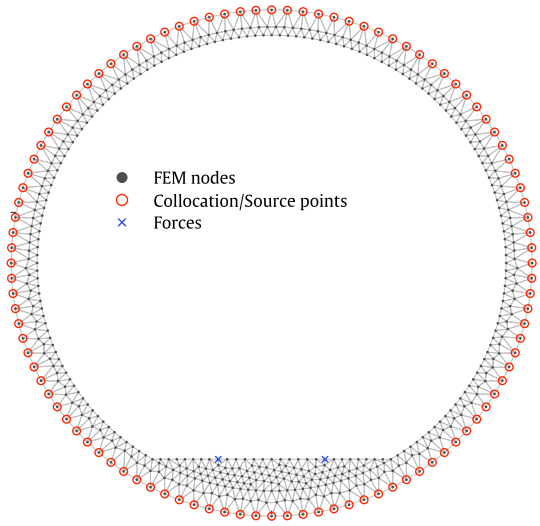

Fig. 13. FEM mesh for 6 nodes per wavelength along the boundary. The FEM nodes, the collocation/source points and the position of the applied forces used in the case study are also included.

4.2. Results

In this section, the response of the tunnel-soil model previously described is presented. The results are presented in terms of response at the evaluation points A and B for each one of the three numerical methods compared in previous sections: 2.5D FEM–SBM, 2.5D FEM–MFS and 2.5D FEM–BEM. For the 2.5D FEM–BEM, the FEM mesh with 6 nodes per wavelength along the boundary has been used. For 2.5D FEM–SBM and 2.5D FEM–MFS, both 6 and 8 nodes per wavelength meshes (referred to as 6NpW and 8NpW, respectively) are used. The longitudinal wavenumber has been sampled using a logarithmic sampling from 0 to 100 rad/m with 129 points. In the computations using the 2.5D FEM–BEM, two Gaussian points were used in this case. The layered soil Green's functions are computed using the EDT toolbox [36], where the wavenumber associated to the y direction is logarithmically sampled in a range from 10^{-7} rad/m and 10^3 rad/m with a total amount of 2048 values. Convergence tests showed that this number of samples was sufficient to obtain accurate results. In what follows, the soil displacement response caused by the action of the two unit point loads is referred to as receptance.

Fig. 14 shows the receptance at the evaluation points A and B and for y and z components. Based on the results shown in Fig. 14, a generally good agreement is observed between the responses obtained with the proposed approach and those obtained using the other two methods for the case of 6NpW. Comparing the results obtained with the 2.5D FEM–SBM with 6 and 8 nodes per wavelength at the maximum frequency, an adequate convergence of the method is observed. Results start to differ just at 60 Hz, which is consistent with the fact that, above this frequency, the number of nodes per wavelength is going below 10 for the 6NpW case. Regarding 2.5D FEM–MFS, the method shows larger discrepancies between 6NpW and 8NpW cases at large frequencies with respect to the 2.5D FEM–SBM.

5. Conclusions

In this paper, a novel numerical methodology to deal with longitudinally invariant soil–structure interaction problems is proposed. This

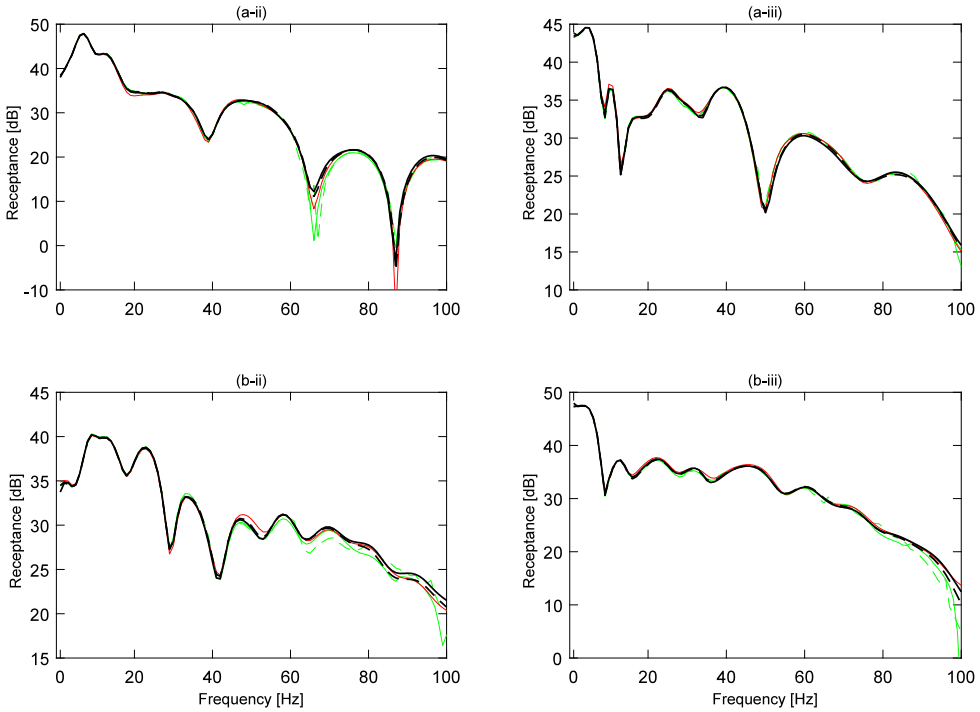

Fig. 14. Receptances at points A (a) and B (b) for y (ii) and z (iii) directions. Methods: 2.5D FEM–BEM [4] 6NpW (solid red line), 2.5D FEM–SBM 6NpW (solid black line), 2.5D FEM–MFS [14] 6NpW (solid green line), 2.5D FEM–SBM 8NpW (dashed black line) and 2.5D FEM–MFS 8NpW (dashed green line). (For interpretation of the references to colour in this figure legend, the reader is referred to the web version of this article.)

approach works in the wavenumber–frequency domain and models the structure with the finite element method and the soil with the singular boundary method. This new approach has been compared with two previously well-established approaches: the 2.5D FEM–BEM [4] and 2.5D FEM–MFS [14]. In general, the results show that the novel approach provides higher accuracy than 2.5D FEM–MFS with a similar computational cost. With respect to the 2.5D FEM–BEM, similar accuracy is reached with larger computational efficiency. The particular merits of the proposed approach are listed as below:

- The approach combines the benefits of the FEM and the SBM, providing the capability for dealing with detailed structures (FEM) and the efficient treatment of the wave propagation in the soil (SBM).
- The method is studied in the framework of simple (a thin cylindrical shell) and more complex (a star-like beam structure) smooth geometries of the soil–structure interface, showing that the proposed method not only is practical for structures with geometrically simple boundaries but also it has reasonable accuracy in cases where the interface is more intricate.
- The convergence analysis carried out has pointed out that the proposed method has an acceptable performance when compared to the other presented approaches at low frequencies while at high frequencies more than 10 nodes per wavelength are required to achieve an acceptable level of accuracy.
- Comparing with the 2.5D FEM–BEM methodology, the computational efficiency of the novel 2.5D FEM–SBM is a great advantage of the method, while exhibiting a similar accuracy considering the same number of nodes per wavelength. Moreover, using SBM strongly simplifies the formulation and implementation of the method.
- Comparing with the 2.5D FEM–MFS approach, 2.5D FEM–SBM is more robust since no virtual boundary is required. This is of special importance for problems with complex geometries for the soil–structure interaction boundary. The overlapping between collocation and source points also allows the method to couple a structure just on the soil surface and keep using half-space Green's functions, a capability that the 2.5D FEM–MFS does not have. This can be used to deal with the soil–structure interaction of several structures such as at-grade railway tracks and roads.
- An example of application for the novel method in underground railway-induced vibration assessment has been presented for a realistic scenario, showing the adequacy of the method for dealing with these kinds of problems.

To conclude, the 2.5D FEM–SBM is found to be an adequate prediction tool for the soil–structure interaction problems since it inherits some of the key advantages of the boundary element method and method of fundamental solutions, while keeping the versatility presented by the finite element method.

CRediT authorship contribution statement

Hassan Liravi: Methodology, Software, Validation, Investigation, Writing – original draft, Writing – review & editing. **Robert Arcos:** Writing – original draft, Writing – review & editing, Supervision, Conceptualization, Visualization. **Arnau Clot:** Writing – review & editing, Supervision, Conceptualization, Visualization. **Kenny F. Conto:** Software. **Jordi Romeu:** Funding acquisition.

Declaration of competing interest

The authors declare that they have no known competing financial interests or personal relationships that could have appeared to influence the work reported in this paper.

Acknowledgements

This research has been carried out with the financial support of Acoustical and Mechanical Engineering Laboratory (LEAM) of the Universitat Politècnica de Catalunya UPC and the project VIBWAY: Fast computational tool for railway-induced vibrations and re-radiated noise assessment, with reference RTI2018-096819-B-I00, supported by the MCIN/AEI/10.13039/501100011033 and FEDER "*Una manera de hacer Europa*". Also, the fourth author would like to thank to the Programa Nacional de Becas y Crédito Educativo PRONABEC (www.pronabec.gob.pe) for the financial support given through the scholarship: "Beca Presidente de la República" from Perú.

Appendix

Eq. (10) can be derived following a procedure similar to the one presented, for example, in [32]. The following direct boundary integral equation for the elastostatic plane strain problem for an interior domain is initially considered [29]:

$$\boldsymbol{U}(\boldsymbol{y}) = \int_{\Gamma} \left[\mathbf{H}^{I}(\boldsymbol{x},\boldsymbol{y})\boldsymbol{T}(\boldsymbol{x}) - \mathbf{H}^{\tau,I}(\boldsymbol{x},\boldsymbol{y})\boldsymbol{U}(\boldsymbol{x})\right] \mathrm{d}\Gamma(\boldsymbol{x}), \quad \boldsymbol{y} \in \Omega^{I}, \tag{A.1}$$

where $\boldsymbol{y}$ is a field point located inside the domain. Substituting the elementary solutions corresponding to rigid-body displacements of the whole body in the direction of each one of the coordinate axes (i.e. $\boldsymbol{U}_1(\boldsymbol{x}) = [1 \quad 0 \quad 0]^T$, $\boldsymbol{U}_2(\boldsymbol{x}) = [0 \quad 1 \quad 0]^T$ and $\boldsymbol{U}_3(\boldsymbol{x}) = [0 \quad 0 \quad 1]^T$ with null tractions, the following expression can be obtained [29]:

$$\int_{\Gamma} \mathbf{H}^{\tau,I}(\boldsymbol{x},\boldsymbol{y})\,\mathrm{d}\Gamma(\boldsymbol{x}) = -\mathbf{I}, \quad \boldsymbol{y} \in \Omega^{I}. \tag{A.2}$$

When the field point $\boldsymbol{y}$ approaches the boundary collocation point $\boldsymbol{y}^m$, Eq. (A.2) can be discretised as follows

$$\begin{aligned}\int_{\Gamma} \mathbf{H}^{\tau,I}(\boldsymbol{x},\boldsymbol{y}^m)\,\mathrm{d}\Gamma(\boldsymbol{x}) &= \sum_{n=1}^{N} \int_{\Gamma_n} \mathbf{H}^{\tau,I}(\boldsymbol{x},\boldsymbol{y}^m)\,\mathrm{d}\Gamma_n(\boldsymbol{x}) \\ &\approx \sum_{n=1}^{N} \mathbf{H}^{\tau,I}(\boldsymbol{x}^n,\boldsymbol{y}^m) L_n, \quad \boldsymbol{y}^m \in \Gamma.\end{aligned} \tag{A.3}$$

where, as before, Γ_n is the segment of boundary on which the nth collocation point is located and L_n is its length. Therefore, it can be seen from Eqs. (A.2) and (A.3) that

$$\sum_{n=1}^{N} \mathbf{H}^{\tau,I}(\boldsymbol{x}^n,\boldsymbol{y}^m) L_n = -\mathbf{I} \tag{A.4}$$

and Eq. (10) can be finally obtained by dividing the previous equation by L_m,

References

[1] Clouteau D, Cottereau R, Lombaert G. Dynamics of structures coupled with elastic media - A review of numerical models and methods. J Sound Vib 2013;332(10):2415–36.
[2] Galvín P, François S, Schevenels M, Bongini E, Degrande G, Lombaert G. A 2.5D coupled FE-BE model for the prediction of railway induced vibrations. Soil Dyn Earthq Eng 2010;30(12):1500–12.
[3] Jin Q, Thompson DJ, Lurcock DEJ, Toward MGR, Ntotsios E. A 2.5D finite element and boundary element model for the ground vibration from trains in tunnels and validation using measurement data. J Sound Vib 2018;422(February):373–89.
[4] François S, Schevenels M, Galvín P, Lombaert G, Degrande G. A 2.5D coupled FE–BE methodology for the dynamic interaction between longitudinally invariant structures and a layered halfspace. Comput Methods Appl Mech Engrg 2010;199(23–24):1536–48.
[5] Ozdemir Z, Coulier P, Lak MA, François S, Lombaert G, Degrande G. Numerical evaluation of the dynamic response of pipelines to vibrations induced by the operation of a pavement breaker. Soil Dyn Earthq Eng 2013;44:153–67.
[6] Hwang RN, Lysmer J. Response of buried structures to traveling waves. Int J Rock Mech Min Sci Geomech Abstr 1981;18(4):73.
[7] Yang YB, Hung HH. A 2.5D finite/infinite element approach for modelling visco-elastic bodies subjected to moving loads. Internat J Numer Methods Engrg 2001;51(11):1317–36.

[8] L. G. Finite element computation of dispersion properties of thin-walled waveguides. J Sound Vib 1994;173(1):113–24.
[9] L. G. Computation of propagative waves in free rail using a finite element technique. J Sound Vib 1995;185(3):531–43.
[10] Sheng X, Jones CJ, Thompson DJ. Modelling ground vibration from railways using wavenumber finite- and boundary-element methods. Proc R Soc A 2005;461(2059):2043–70.
[11] Lopes P, Alves Costa P, Calçada R, Silva Cardoso A, Costa PA, Calçada R, Cardoso AS. Influence of soil stiffness on building vibrations due to railway traffic in tunnels: Numerical study. Comput Geotech 2014;61(November 2017):277–91.
[12] Freisinger J, Hackenberg M, Müller G. A coupled integral transform method - finite element method approach to model the soil structure interaction of finite (3D) and length invariant (2.5D) systems. J Sound Vib 2020;482.
[13] Tadeu A, António J, Godinho L. Defining an accurate MFS solution for 2.5D acoustic and elastic wave propagation. Eng Anal Bound Elem 2009;33(12):1383–95.
[14] Amado-Mendes P, Alves Costa P, Godinho LM, Lopes P. 2.5D MFS-FEM model for the prediction of vibrations due to underground railway traffic. Eng Struct 2015;104:141–54.
[15] Liravi H, Arcos R, Ghangale D, Noori B, Romeu J. A 2.5D coupled FEM-bem-MFS methodology for longitudinally invariant soil-structure interaction problems. Comput Geotech 2021;132(February):104009.
[16] Young DL, Chen KH, Lee CW. Novel meshless method for solving the potential problems with arbitrary domain. J Comput Phys 2005;209(1):290–321.
[17] Liu L. Single layer regularized meshless method for three dimensional exterior acoustic problem. Eng Anal Bound Elem 2017;77(April):138–44.
[18] Liu Y. A new boundary meshfree method with distributed sources. Eng Anal Bound Elem 2010;34(11):914–9.
[19] Kim S. An improved boundary distributed source method for two-dimensional Laplace equations. Eng Anal Bound Elem 2013;37(7–8):997–1003.
[20] Chen W, Wang F. A method of fundamental solutions without fictitious boundary. Eng Anal Bound Elem 2010;34(5):530–2.
[21] Wei X, Chen W, Sun L, Chen B. A simple accurate formula evaluating origin intensity factor in singular boundary method for two-dimensional potential problems with Dirichlet boundary. Eng Anal Bound Elem 2015;58:151–65.
[22] Chen W, Gu Y. An improved formulation of singular boundary method. Adv Appl Math Mech 2012;4(5):543–58.
[23] Chen W, Fu Z-J, Wei X. Potential problems by singular boundary method. Comput Model Eng Sci 2009;(February 2015).
[24] Pang G, Chen W. Symmetric singular boundary method for potential problems with mixed boundary conditions. Eng Anal Bound Elem 2015;56:49–56.
[25] Fu ZJ, Chen W, Gu Y. Burton-Miller-type singular boundary method for acoustic radiation and scattering. J Sound Vib 2014;333(16):3776–93.
[26] Fu Z, Chen W, Wen P, Zhang C. Singular boundary method for wave propagation analysis in periodic structures. J Sound Vib 2018;425:170–88.
[27] Wei X, Luo W. 2.5D singular boundary method for acoustic wave propagation. Appl Math Lett 2021;112:106760.
[28] Fu Z, Xi Q, Li Y, Huang H, Rabczuk T. Hybrid FEM–SBM solver for structural vibration induced underwater acoustic radiation in shallow marine environment. Comput Methods Appl Mech Engrg 2020;369:113236.
[29] Gu Y, Chen W, Fu ZJ, Zhang B. The singular boundary method: Mathematical background and application in orthotropic elastic problems. Eng Anal Bound Elem 2014;44:152–60.
[30] Fu ZJ, Chen W, Chen JT, Qu WZ. Singular boundary method: Three regularization approaches and exterior wave applications. CMES - Comput Model Eng Sci 2014;99(5):417–43.
[31] Sun L, Chen W, Cheng AH. Singular boundary method for 2D dynamic poroelastic problems. Wave Motion 2016;61:40–62.
[32] Gu Y, Chen W, Zhang J. Investigation on near-boundary solutions by singular boundary method. Eng Anal Bound Elem 2012;36(8):1173–82.
[33] Dineva PS, Manolis GD, Wuttke F. Fundamental solutions in 3D elastodynamics for the BEM: A review. Eng Anal Bound Elem 2019;105(April):47–69.
[34] Tadeu A, António J, Godinho L. Green's function for two-and-a-half dimensional elastodynamic problems in a half-space. Comput Mech 2001;27(6):484–91.
[35] Ghangale D, Colaço A, Alves Costa P, Arcos R. A methodology based on structural FEM-BEM and acoustic BEM models in 2.5D for the prediction of re-radiated noise in railway-induced ground-borne vibration problems. J Vib Acoust 2019;141(June):1–14.
[36] Schevenels M, François S, Degrande G. EDT: An ElastoDynamics toolbox for MATLAB. Comput Geosci 2009;35(8):1752–4.
[37] Noori B, Arcos R, Clot A, Romeu J. A method based on 3D stiffness matrices in Cartesian coordinates for computation of 2.5D elastodynamic green's functions of layered half-spaces. Soil Dyn Earthq Eng 2018;114(March):154–8.
[38] De Oliveira Barbosa JM, Kausel E, Azevedo A, Calçada R. Formulation of the boundary element method in the wavenumber-frequency domain based on the thin layer method. Comput Struct 2015;161:1–16.
[39] Chen W, Lin J, Chen CS. The method of fundamental solutions for solving exterior axisymmetric helmholtz problems with high wave-number. Adv Appl Math Mech 2013;5(4):477–93.
[40] Chen CS, Karageorghis A, Li Y. On choosing the location of the sources in the MFS. Numer Algorithms 2016;72(1):107–30.
[41] Forrest JA, Hunt HEM. A three-dimensional tunnel model for calculation of train-induced ground vibration. J Sound Vib 2006;294(4–5):678–705.
[42] International Organization for Standardization. ISO 14837-1. Mechanical vibration. Ground-borne noise and vibration arising from rail systems. Part 1: General guidance. 2005.